Effective separation of Oil-in-Water using exfoliated g-C3N4- PSf composite membranes

R. Geetha Balakrishna (br.geetha@jainuniversity.ac.in)
Jain University
Swathi Divakar
Jain University
Prajwal Sherugar
Jain University
K.K. Nagaraja
Manipal Institute of Technology https://orcid.org/0000-0001-5449-4075
Dr Mahesh Padaki
Centre for Nano and Materials Sciences, Jain University

Article

Keywords: Graphitic carbon nitride, oil- water separation, polysulphone

Posted Date: August 18th, 2022

DOI: https://doi.org/10.21203/rs.3.rs-1862203/v1

Abstract

Integrated membranes are found to have tremendous application in treating oily waste water to produce potable water. The present work reports the use of graphitic carbon nitride (g-C_3N_4) as a suitable membrane additive mainly because of its hydrophilic nature and strong functionality. Exfoliated g-C_3N_4 offers high surface area and more active centres required for membrane applications. This work demonstrates the excellent features observed on exfoliation of g-C_3N_4 as a composite material in polysulphone (PSf) membranes. The well thought out exfoliated g-C_3N_4-PSf composite gave promising oil-water separation with oil rejection >99%. In addition, these exfoliated laminar planes interacted well with the polymer giving both thermally and mechanically stable membranes. The membrane also attains high porosity, enhanced hydrophilicity and adequate oily water treatment ability. Oil being the important fouling component can easily destroy membranes if not addressed. This fouling behaviour of membrane is tackled where the composite membrane shows a remarkable flux recovery ratio of near 100% with no comprise in oil rejection during subsequent cycles. This current study demonstrates high porosity, enhanced hydrophilicity and adequate oil-water treatment ability. The study does provide insights into the use of such nanosheets to achieve good chemical interaction with the membrane matrix thus providing the synergistic features of both g-C_3N_4 and PSf.

1. Introduction

Anthropogenic activities are the main cause for release of oil into marines and accumulation of oily-water content in the environment. A typical of 140,000 liters of water is being contaminated by oil during mining every day. In addition, many industries such as textiles, petrochemicals, metal and steels etc., generate huge volumes of oil either as an essential commodity or as oily-wastewater which contributes tremendously to oil-water pollution and is currently an environmental crisis[1]. Oil spill incidents and high oily waste water released from industries have caused adverse and catastrophic influence on aquatic ecosystem and also led to huge financial loss[2]. Although this concern has led to a decline in the number of heavy oil-spills (> 700 tones) over the last decade[3], yet the quantum of oily waste being generated is still very high. In the year 2020, oil spills of 7-700 tons were recorded for 3 times with approximately 1,000 tons of oil being released to the environment.

The most common treatment techniques used as remediation for oil-water separation are: filtration and adsorption involving materials such as mesh[4], fillers[5], membranes[6], films and porous media, powder, particles, gel and nano-composites respectively[1]. Initially the main moto of membrane technology was to ensure potable water, wherein every membrane material was designed keeping this in mind. But now this technology has extended its wings in all fields of science and proven its capabilities. Membranes with smart materials have attracted high interest in research for separation of oil from water. Smart hybrid materials with super-wettability are desired for efficient oil-water separation[7]. Many factors such as the membranes porosity, breakthrough pressure, surface interactions, hydrophilicity and antifouling behavior determine their performance and ability to achieve separation. Polysulphone (PSf) in specific is found to

have remarkable features despite its low-cost, of which strong thermal stability, mechanical properties, enhanced chemical stability for instance, strongly labile in oxidizing, acidic and basic environment are of prominent importance[8].

However, PSf is relatively hydrophobic which is undesirable property with respect to the membrane separation intended in this study. Hence, in order to dominate this nature, hydrophilic additives are chosen. The hydrophilic additive used here in this work is graphitic carbon nitride (g-C_3N_4) for oil-water separation[9]. g-C_3N_4 is found to be a fascinating carbon material due to its unique physicochemical features. The layered structures of g-C_3N_4 are connected to each other by Van der Waals force of attraction due to the π-π-stacking that is observed between the triazine ring systems. These ring systems consist of sp^2 hybridized C-N bond forming an aromatic π-conjugation[10]. This structural feature of g-C_3N_4 ensures thermochemical stability in both acidic and basic pH. On comparing the inherent physio-chemical properties of g-C_3N_4 with other 2D materials: graphene oxide (GO) also being a 2D material is susceptible to swelling due to the presence of hydrophilic functionalities such as hydroxyl groups, carbonyl, epoxy etc[11], on the other hand 2D materials for example, metal organic framework and covalent organic framework also face the same hurdle. Though molybdenum sulphide (MoS_2) shows superior properties than GO, MOF and COF in membrane technology it has a major drawback in terms of porosity, where small molecules travel a strenuous path which eventually hinders separation ability of the material[12]. On evaluating the above-mentioned obstacles, g-C_3N_4 is found to rationale in all aspects and is therefore a suited candidate for membrane-based separation.

g-C_3N_4 -PSf is thus envisaged as one such couple that is compatible in terms of stability (promised by PSf) and chemical nature (ensured by g-C_3N_4). g-C_3N_4 can hence be considered a hotspot additive for development of smart membranes. This is due to the adjustable surface property, high porosity, stability and rigid porous structure it renders to the membranes when compared to other porous materials. More than all, the major advantage of graphitic carbon nitride is its hydrophilic nature, which plays a vital role in membrane technology since it alleviates membrane fouling and enables rapid diffusion of water through the membrane matrix which confers improved performance of the membrane[13].

Alias et al, have fabricated g-C_3N_4 embedded electro spun polyacrylo nitrile (PAN) membranes for photocatalytic degradation of oil with oil removal by only 85.4% [14]. Similarly, another group synthesized homogenously distributed $AlSi_2O_6$ nanoparticle on PSf matric for oil water separation and achieved a separation up to 97% with reasonably high flux[6]. From the mentioned literature it is evident that usage of membrane materials such like PAN have been used with g-C_3N_4 [15] where PAN would not meet the economic demands. Also exfoliated g-C_3N_4 is found to have an upper hand when compared to bulk g-C_3N_4 in terms of higher surface area, increasing the active sites and lesser energy band gap[16,17]. With this motivation and on carrying out an unbiased literature survey we have showed the first-time use of exfoliated g-C_3N_4 to achieve high oil rejection and elevated percentage of flux recovery ratio (with no compromise in rejection), though there was concession on the flux obtained. However, this study

investigated the impact of hydrophilicity and pore size. The surface and the core structure of the pristine and the modified membrane material were characterized using various spectroscopic and microscopic techniques. Hydrophilicity and porosity were evaluated experimentally, water uptake, contact angle, pure water flux studies which helps its correlation to oil-water separation and antifouling properties of the membrane. The study also offers the structural elucidation of chemical interaction between exfoliated g-C_3N_4 and surface of PSf membrane that facilitates these enhanced properties.

2. Experimental Section

Melamine ($C_3H_6N_6$), Sulphuric acid from Sigma Aldrich, 1-methyl-2-pyrrolidone (NMP) purchased from Sigma Aldrich, Polysulphone (PSf-35000 Da) commercial, Sodium dodecyl sulphate (SDS) from Merck. Machine oil (90% of pure base oil and remaining 10% of the additives, which possesses the density of about 881.4 kg/m^3 at 25°C) from Bangalore, India. The chemicals used in the study were as reagent grade therefore no further purification was needed.

2.1. Preparation of graphitic carbon nitride

In brief, 20g of white melamine powder was placed in a silica crucible with lid and heated at 550°C for 4 hours in the muffle furnace. After the completion of calcination, the vessel was cooled to room temperature after which the yellow g-C_3N_4 product was ground and used for further use[13]. Then 5g of g-C_3N_4 powder was mixed with 10mL of sulphuric acid (98 wt%) in a 50mL standard flask and kept for stirring at room temperature for 8 hours. Then the mixture was transferred slowly into a vessel containing 100mL distill water and sonicated to achieve exfoliation. The temperature of the reaction vessel increases drastically on account of energy release and eventually led to color change from yellow to white. The obtained suspension was then centrifuged, washed thoroughly to eliminate unexfoliated g-C_3N_4 and later centrifugation was continued to neutralize the excess acid. Finally, the obtained product was dried overnight at 80°C[18]. The procured exfoliated g-C_3N_4 was labeled as Eg-C_3N_4

2.2. Fabrication of mixed matrix membrane

The Eg-C_3N_4-PSf mixed matrix membrane were synthesized by Diffusion Induced Phase Separation (DIPS) process. This was achieved by preparing varied concentrations of PSf and Eg-C_3N_4 which was used to check the membranes performance. Initial, required quantity of Eg-C_3N_4 was added to 16mL of NMP and sonicated to obtain a uniform dispersion of particles, to this mixture a specific weight of PSf was added gradually at room temperature for 24 hours to achieve a homogenous casting solution. Later the viscous casting solution was degassed for an hour without any agitation. Finally, the polymeric solution was dispersed uniformly onto the glass plate and the solution was casted using a glass rod. The casted membrane was later dipped into the coagulation bath containing the nonsolvent at room temperature to initiate phase separation. After the membrane peeled off from the glass plate and the membrane was transferred to another water bath for 24 hours to remove any residual solvent if any[6]. The

concentration of Eg-C_3N_4 used was categorized into 3 segments low (2.5%), high (5%) and very high (7.5%). These concentrations were chosen due to its enhanced hydrophilicity and stability. The membrane compositions are as tabulated in Table 1.

Table 1
Different composition of the synthesized composite membranes

Name of the membrane	Eg-C_3N_4 (g)	PSf (g)	NMP (mL)
M (PSf)	0	4.0	16
M_1 (2.5% g-C_3N_4-PSf)	0.1	3.9	16
M_2 (5% g-C_3N_4-PSf)	0.2	3.8	16
M_3 (7.5% g-C_3N_4-PSf)	0.3	3.7	16

3. Characterization Of G-cn And Composite Membranes

The characterization instrument details used to evaluate the physical and chemical properties of the additive and composite membranes are outlined in **Supplementary Information**.

4. Performance Study Of The Membrane

Formulas pertaining to porosity, pore size, water uptake, pure water flux, permeability, rejection, flux recovery ration and types of fouling are provided in the **Supplementary Information.**

5. Results And Discussion

5.1 Characterisation of g-C_3N_4

Figure 1a shows the X-Ray Diffraction (XRD) patterns of Eg-C_3N_4. The recorded XRD pattern of the bulk g-C_3N_4 matched with JCPDS file 87-1526 and also with reported literature[19,20,21]. The 2θ values at 27.73° and 12.72° corresponds to the hkl plane 002 and 100 attributed to interlayer stacking of the heterocyclic aromatic ring and in-plane structure of tris-triazine unit of graphitic carbon nitride respectively. The slight peak shifts to lower theta indicates wider packing and decrease in intensity of 002 peak and arise of many new peaks in exfoliated g-C_3N_4 can be attributed to the delamination of planes and enhanced disordered layers of the exfoliated structure, thereby confirming successful exfoliation of the g-C_3N_4[22].

The Brunauer-Emmett-Teller (BET) adsorption-desorption isotherms of Eg-C_3N_4 were carried out and it depicted a significant type-II isotherm hysteresis curve, which corresponds to mesoporous nature of Eg-C_3N_4 and the surface of the material was found to have a surface area of 14.9m^2/g and 23.72m^2/g for bulk and exfoliated respectively. The larger BET surface area of exfoliated g-C_3N_4 is attributed to

destruction of assembly of in-plane aromatic system by H_2SO_4 treatment which causes change in colour from yellow (bulk g-C_3N_4) to milky white (exfoliated g-C_3N_4)[23]. Mean pore volume of 0.048553cm^3/g and a mean pore diameter of 8.18nm obtained is in good agreement with the literature[24]. Since the pore size gives us the information that Eg-C_3N_4 is mesoporous in nature, we can conclude that the porosity of materials is much less than the oil droplet size (micrometre range) and can be used in oily waste water treatment.

The surface morphology of the synthesised bulk and exfoliated g-C_3N_4 was characterised by Field Emission Scanning Electron Microscope (FESEM) and the images are provided in Fig. 2. The stacked and agglomerated g-C_3N_4 nanosheets have successfully been exfoliated into layers as observed in Fig. 2.

5.2 Fourier Transform-Infrared (FT-IR) results of g-C_3N_4

FT-IR analysis of Eg-C_3N_4 is shown in Fig. 1 **(b)** which depicts the characteristics peaks of graphitic carbon nitride. For instance, peaks at 1242, 1320 and 1403 cm^{-1} are due to stretching of aromatic C-N group and finally the peak at 1636 cm^{-1} attributes to C-N stretching. One can conclude the retention of all the functional groups except for 795 cm^{-1} peak which shows a shift to 814 cm^{-1} with a significant increase in intensity indication enhanced vibration of tris-s-triazine on exfoliation. The enhanced peak in the region at 3100 cm^{-1} correlates with the N-H stretching indicating more number of uncondensed terminal 'N' groups [18,25].

5.3 Membrane Characterisation

5.3.1 Structural study of Eg-C_3N_4-PSf membrane using XRD and PSf

Figure 3 shows the XRD pattern of Eg-C_3N_4 nanosheets, pristine PSf (control) and the fabricated Eg-C_3N_4-PSf membrane. A broad peak for pristine PSf is observed at a 2θ range of 17.9° [26]. Composite membranes M_1, M_2 and M_3 shows all the peaks corresponding to pristine PSf and Eg-C_3N_4. It was also observed that, the amorphous PSf peak attains crystallinity in the composite membrane because of the intercalation between Eg-C3N4 and PSf. All the peaks corresponding to Eg-C3N4 appears significantly shifted with complete change in their intensities. As per the reported literature, intensity of 002 peak of Eg-C_3N_4 is found to be very less due to decrease in Eg-C_3N_4 dosage concentration[27] but however we opine that the different arrangement of laminar planes due to its intercalation with the polymer during membrane casting causes these changes in peaks shifts and their intensity[28]. Intensity of these (indicated by *) increases with increase in Eg-C_3N_4 indicating those peaks to be of crystalline g-C_3N_4.

5.3.2 Attenuated Total Reflection-Infrared (ATR-IR) Analysis

The ATR-IR spectra of the membranes are provided in Fig. 4. Peaks corresponding to both g-C_3N_4 and PSf can be found in the composite membrane. Few of the prominent transmittance bands of pristine PSf at

1298, 2966 and 834 cm^{-1} corresponds to sulphonyl group (O = S = O), C-O-C group and aromatic C-H stretching respectively [29,30]. The slight shift in O = S = O stretching of composite membranes peak from 1298 cm^{-1} to 1318 cm^{-1} could be due to hydrogen bonding between sulphonyl group and N-H groups of Eg-C_3N_4. The absence of 3189 cm^{-1} in composite membrane indicates no free amine groups unlike Eg-C_3N_4. The shift of C = C of 1,4 substituted aromatic ring 834 cm^{-1} to 832 cm^{-1} confirms the π-π interactions between PSf ring and the s-triazine heterocyclic ring of Eg-C_3N_4. And also, there is no s-triazine heterocyclic ring peak in composite membrane which could be due to the mentioned interaction. Appearance of peak at 1744 cm^{-1} for N-H stretching in composite membrane is a clear indication of presence of Eg-C_3N_4 but in intercalation with PSf. All other peaks of PSf remain undisturbed and most of the peaks overlap with Eg-C_3N_4. Figure 5 depicts this possible interaction between PSf and Eg-C_3N_4. The presence of π-conjugation in both the polymer matrix and the additive (Eg-C_3N_4) paves way for π-π interaction which could be the driving force behind holding the two cyclic systems together. Another predominant interaction that one can observe is the hydrogen bonding between the oxygen in sulphonyl groups of the PSf material and the hydrogen attached to the electronegative nitrogen in the heterocyclic ring system of Eg-C_3N_4.

5.3.3 Membrane morphology study

The surface images and cross-sectional morphology of the membrane is shown in **Fig S1** and Fig. 6 respectively where Fig. 6a corresponds to the cross-sectional image of pristine PSf and Fig. 6b-6d belongs to various concentrations of Eg-C_3N_4 which provides a cascaded structure to the membrane matrix. The membrane is found to have three distinctive layers, the top layer which accounts for selectivity and rejection, middle layer consisting of finger like layers ensuring productivity and the bottom layer which confers mechanical strength to the membrane. From the FESEM images it is evident that the spongy layer of the pristine PSf membrane is very thick while compared to Eg-C_3N_4 -PSf due to sluggish diffusion of solvent and nonsolvent in pristine PSf. The composite membrane is found to have evident finger like projections in the middle layer and these projections increase with increase in Eg-C_3N_4 concentration in the casting solution and the size of the macrovoids shrink in turn reducing the thickness of the bottom layer. This can be correlated with the cross section of FESEM **(**Fig. 6**)** which shows short thickness of the bottom layer and increase in porosity of the membrane which could adversely weaken the membranes mechanical stability [31]. The incorporation of hydrophilic nanoparticle, accelerates the rate of solvent-nonsolvent exchange during the phase inversion process due to the enhanced interaction between nonsolvent (water) and Eg-C_3N_4 molecules when compared to PSf thus, due to the affinity between water molecules in the coagulation bath and Eg-C_3N_4, limited interaction is observed between the polymer (PSf) and water, the solvent moiety i.e., NMP easily diffuses out into the coagulation bath. This phenomenon contributes to the high porosity of the membrane with increase in concentration of the additive (Table 1) [32].

Another fascinating observation is appearance of the broad finger like projection and large pores in the bottom layer though the size of the layer is reduced. These structural changes are observed also due to

the above-mentioned reason. These structures enhance the membrane properties like porosity, water uptake, stability sufficiently. However optimum concentration of Eg-C3N4 is important as any concentration above that adversely affects properties as aforesaid. The elemental mapping of the membranes are provided in supplementary information **(Fig S2)**.

6. Surface And Mechanical Property Of The Membrane

6.1. Surface Morphology of the Membranes

The topography of membranes was observed using atomic force microscopy (AFM) (Fig. 7). According to the AFM results the surface roughness of the membrane was found to decrease with increase in Eg-C_3N_4 concentration in the casting solution, which is similar to the previous reported literature [32]. We presume the reason for this trend to be due to the 2D sheets like structure of Eg-C_3N_4 which move up to the membrane's surface during phase inversion and leading to diminished surface roughness compared to pristine PSf. It is evident that the hydrophilic fillers tend to move to the membrane surface during phase inversion processes since these additives are sheet like in nature, they give rise to less peaks/valleys that account for surface roughness. However, increase in concentration of additive increases the roughness and beyond optimum amount it reduces the roughness. Exfoliated g-C_3N_4 would reaggregate beyond optimum concentration due to its low surface energy and this can bring down the roughness. However, the phenomenon is found to be random and uncontrollable. The accountability of fouling with respect to surface roughness is explained in the later section **(Sec 6)**.

6.2. Effect of Eg-C_3N_4 on mechanical properties of the membrane

Tensile strength is one important parameter to determine the mechanical property of the membrane. The effect of graphitic carbon nitride dosage on the tensile strength of PSf is shown on Table 2. From this table it is evident that on increasing the concentration of Eg-C_3N_4 in membrane matrix the tensile strength of the membrane is found to increase initially and decreases up to 3.85MPa when the concentration of additive exceeds optimum amount as in membrane M_3. As reported in previous literature, the increase in tensile strength initially can be because of the enhanced interfacial interaction between the polymeric membrane material and additive used [33]. The results emphasis that the tensile strength of the membrane can be tunned on adding a suitable filler based on the requirement. However, keeping in mind, the hurdles caused on increasing the dosage beyond optimum limit we conclude M_2 as the optimum as any concentration of the additive further hampers the mechanical strength of the membrane. AFM and FESEM study also substantiate the need for optimum concentration to achieve enhanced properties as in M_2 composite membrane.

6.3. Water uptake, porosity and contact angle of the membrane

The water uptake, wettability and porosity of the three synthesised membrane along with pristine PSf were evaluated and the results are as provided in Table 2. It is observed that on increasing the dosage of Eg-C_3N_4 the contact angle of the membrane decreases from 64.8° to 52.65° indicating the enhancement in the hydrophilic nature of the material.

From water uptake studies one can understand the absorption capacity and solvent stability of the membrane under consideration. It is noticed that the water uptake capacity of pristine PSf is less when compared to Eg-C_3N_4 membranes which is due to the hydrophobic nature of the pristine membrane and high-water absorption resistance of the plain PSf membrane. From Table 2 we can come to a conclusion that, the water uptake capacity is found to increase with increase in g-C_3N_4 concentration in the membrane matrix. Therefore, the hydrophilic additive i.e., Eg-C_3N_4 facilitates enhanced water absorption capacity and high-water affinity.

Table 2
Contact angle, Water uptake, Porosity and Mean pore radius of various composite membranes

Name of the membrane	Contact angle (°)	Water Uptake (%)	Porosity (ε) (%)	Tensile Strength (MPa)	Mean pore radius (nm)
M (PSf)	64.89	42.23 ± 1.68	46.13	4.61	1.81
M_1 (2.5% g-C_3N_4-PSf)	58.02	61.78 ± 2.36	48.38	4.82	2.81
M_2(5% g-C_3N_4-PSf)	55.08	66.16 ± 1.68	64.07	6.42	3.01
M_3 (7.5% g-C_3N_4-PSf)	52.65	71.34 ± 1.24	76.02	3.85	3.31

6.4 Zeta Potential of the fabricated membranes:

Zeta potentials is one major characterisation technique required to assess the charging behaviour of the membrane when in contact with contaminant solutions. Incorporation of hydrophilic moiety such as Eg-C_3N_4 with functionalities such as amine groups tend to increase the overall net negative charge on the membrane surface. The factors which govern this behaviour are the surface composition, solution pH and the ionic strength which imposes charge on the membrane. From the zeta potential studies (Fig. 8), it is evident that, the potential decreases (more negative) with increase in pH.

The zeta potential of pristine PSf is itself negative due to presence of sulphonic groups which gets protonated resulting in cationic absorption at low pH therefore the increase in zeta potential with decrease in surface charge at low pH is expected[34]. The significant decrease in zeta potential for

composite membranes is due protonation of the nitrogen (containing lone pair) in graphitic carbon nitride which eventually carries positive charge hence the membrane has less negative charge at acidic pH, where as in basic pH even the sulphonyl groups remain deprotonated thereby rendering high negative charge on the membrane. In M_3 membrane the zeta potential was found to showcase a slight increase in potential which attributes to the agglomeration of the hydrophilic additive on the surface of the membrane which in turn reduces the surface functionality of the additive on the membrane[35]. Since the membrane has an overall negative charge over a wide pH range including the biological pH, the rejection of oil is thereby enhanced as the emulsifier used is negatively charged (electrostatic repulsion).

6.5. Thermogravimetry Analysis (TGA):

Thermal stability of the membrane is one of the important parameters to evaluate the possibility of real time separation. Figure 9 shows TGA of plain PSf and the corresponding composite membranes of Eg-C_3N_4-PSf.

Profuse material loss in the temperature range of 500° C to 650° C was observed in both pristine and composite PSf due to the thermal decomposition of membrane skeleton. Addition of Eg-C_3N_4 into the membrane matrix lowers the thermal stability of membrane matrix due to chemical interaction between the two, which are weak and does not withstand this temperature. The rapid weight loss in composite membrane can also be due to the same decomposition temperature of Eg-C_3N_4 as well [36, 37, 38] .

7. Separation Strategy Of G-c3n4 Based Membranes And Oil-water Separation Theory

Irrespective of the fabrication method imbibed in synthesis of Eg-C_3N_4 membrane the arrangement of Eg-C_3N_4 in the membrane can be divided into: laminar and mixed matrix membranes.
A regular laminar type membrane is where the Eg-C_3N_4 is stacked via parallel-nanosheets on a porous substrate through vacuum assisted or pressure driven or dip coating methods. There are common pathways by which small molecules (during separation) diffuses through the laminates, such as the gaps between the nanosheet edges, nanochannels present between the interlayers of the sheet edge and basal plane of the adjacent Eg-C_3N_4 sheets, intrinsic triangular nanopores and amidst the defects on the Eg-C_3N_4 structural plane. It is also observed that the small molecules diffuse easily across the laminar structure of the membrane and reject the larger molecules. It is practical that the diffusion of water along the laminates is different when compared to other smaller contaminants (in this study). Few studies show that diffusion of water occurs through ultra-low friction. It is this nano-fluidics that allow good permeability of water in the laminates of Eg-C_3N_4.

In case of a mixed matrix membrane, the incorporation of Eg-C_3N_4 alters the regular interchain packing of the polymer in the membrane leading to the formation of Eg-C_3N_4 /polymer interfacial voids. These voids mimic as extra nanochannels that aid in non-selective molecular transport. It is evident that Eg-C_3N_4 enhance the selectivity of the membrane by changing the morphology and surface characteristics of the

membrane. It is also proven that the hydrophilic nature of Eg-C_3N_4 allows easy penetration of water molecules across the membrane which is also observed in this study. The pore structure formed due to loading of Eg-C_3N_4 in the phase inversion process dominates the separation process over the polymeric pores[13] .

Surfactants are prone to alter both, features of the emulsion created and the membrane's wettability and surface charge. When the surfactant segregates from water and enters the oil-water interface, the surfactant decreases the oil-water interfacial tension and in turn reduce the energy necessary to break the droplet. The speciality of the surfactant employed depends on the concentration, type of surfactant, mixing conditions, temperature and the composition etc. The emulsion's charge is majorly influenced by the surfactant used, for instance if the surfactant used is positive in charge the zeta potential of the emulsion is positive at neutral pH, on the other hand if the emulsifier (surfactant) used is negatively charged like (sodium dodecylsulphate (SDS)) then the overall zeta potential of the emulsion is negatively charged. When porous polymeric membranes are used to separate oil-water emulsions, the oily phase under some circumstances can enter the membrane pores. These conditions are governed by the properties of the emulsion (droplet size, interfacial tension etc), membrane pore size, membrane morphology, transmembrane pressure etc. Say for instance the oil-droplet size is lesser in dimension when compared to nominal membrane pore size ($d_{drop} << d_{pore}$), the oil drifts easily across the membrane matrix causing intrapore fouling. Therefore, in order to avoid intrapore fouling membranes must be fabricated such that the membrane pore size must be lesser than the oil droplet size. Under these circumstances the oil rejection cannot be 100% guaranteed if the transmembrane pressure is higher[39]. In this study since the membrane is negatively charged at a wide pH range the usage of anionic surfactant is more apt and advisable for easy rejection due to repulsive forces. On extrapolating the theory to this study, the emulsifier used here is anionic surfactant, sodium dodecyl sulphate. Since the surfactants charge is negative it renders an overall negative charge to the oil-water emulsion. And the membrane on the other hand being negatively charged repels the oil emulsion and enabling rejection. Another key factor that needs to be kept in mind is the pore size of the membrane **(Table S1)** as the membrane's pore size is within the nanometre range and the size of the oil emulsion is in micrometre range, ($d_{drop} >> d_{pore}$) size influenced rejection is also a possibility.

8. Membrane Performance Study

Permeation, rejection and antifouling study of the membrane

The pure water flux and oil-rejection of the Eg-C_3N_4 -PSf membrane are represented in Fig. 10. It is evident from the study that pure water flux for pristine PSf is significantly less than Eg-C_3N_4 -PSf membrane which attributes to the enhanced hydrophilicity of Eg-C_3N_4 additive that is incorporated into the membrane as shown in Fig. 10a. There is a slight deviation from normality i.e., the water flux of M_2 membrane was found to be greater than M_3 membrane at higher pressure range though the concentration of additive is greater in the later which can be due to surface pore blockage of the

membranes by Eg-C_3N_4 sheets due to its higher concentration. Increase in resistance towards mass transfer (due to pore blockage) reduces effective active sites of the additive [40,41].

In case of rejection studies, 1000ppm oil-water emulsion was prepared and chosen as the feed solution. 0.1g/L of SDS was added as the surfactant in order to decrease interfacial tension to achieve droplet formation and eventually yield small oil droplets (Fig. 11) with enhanced stability[39]. The rejection percentage of oil by the prepared membranes are represented in Fig. 12. It is observed that the Eg-C_3N_4 -PSf shows ≈100% rejection when compared to pristine PSf membrane with ≈ 50% rejection over a pressure range of 2bar-6bar and over a period of 360 minutes. Induced hydrophilicity by Eg-C_3N_4 facilitates oil droplets to be rejected or repelled from the membrane surface resulting in high oil rejection. Another evident reason for enhanced oil rejection ability of the membrane can be attributed to the pore size of the membranes M_1, M_2 and M_3 (Table 2). Since the membrane pore size lies within nanometre range and the oil droplet size is in micrometre range, it can be substantiated that the oil rejection could be even due to smaller membrane pore size compared to oil droplet size **(membrane pore size calculations are provided in the Supplementary Information)**.

From Fig. 10b it is manifested that there is a slight decline in flux while moving from pure water to oil-water emulsion for M_3 membrane and this is attributed to the increase in viscosity of the oil-water solution. From long term study as shown in Fig. 14, it is observed that the membranes were weakly fouled by oil which accounts for the flux decline and it is also evident that composite membranes show a promising Flux Recovery Ratio (FRR) of 99.4% owing to high antifouling nature of the membrane showing prospects of real time applications and is found to be quiet high compared to other membranes in literature (Table 3). After every run the membranes were washed in a solution containing SDS and stirred for 2 hours at 40°C and guaranteed easy elimination of the weakly bound oil. Later the washed membranes were used for further studies. From “valley clogging theory” it is proven that with enhanced surface roughness, particles preferentially accumulate in the crevice of the valley, therefore with rate of antifouling being proportional to the membrane’s surface roughness. Based on this theory the obtained results for various membranes are in good agreement with the AFM and FRR studies. M_1 membrane is found to have the least surface roughness of 5.52nm (Fig. 6) and hence showing less fouling when compared to M_2 and M_3, though the latter two membranes also showed a comparatively high FRR of 83% and 91% respectively. Therefore, from the obtained results one can conclude that the membranes M_1, M_2 and M_3 offered a high FRR and antifouling property [42, 43].

Even though there is minimal amount of fouling observed, membranes fouling can be categorised into reversible (Rr) and irreversible fouling (Rir). In reversible fouling, the foulants are weakly adhered to the membrane surface and can therefore be easily washed off with water. Likewise, when the foulants which accumulate and interact strongly with the membrane surface are challenging to eliminate even on washing and such fouling is referred to as irreversible fouling. Figure 13 shows the FRR, Rt, Rr and R_{ir} of M_1, M_2 and M_3 membrane. It was observed that Eg-C_3N_4 -PSf shows a promising resistance towards oil-

fouling and can be attributed to the hydraulic layer formed on the membrane surface which would probably also contribute to enhance the rejection capacity of the membrane.

The overall fouling resistance is found to be lesser for M_1 membrane compared to M_2 and M_3 and the irreversible resistance of all the prepared composite membranes are found to be minimal. From the tabulated data it is evident that reversible fouling is slightly pronounced in M_2 (11.98%). So it is in line with literature which reports that hydrophilic membranes are less susceptible to fouling and secondly the membrane fouling is less pronounced when the surfactants are used more so when membrane surface and emulsion carry same charge, thus repelling each other [39]. However, FRR, reversible fouling, irreversible fouling and total fouling ratio are less when compared to earlier reports involving oil-water separation as displayed in Fig. 13d and the outcome of this work is exceptionally good. The incorporation of Eg-C_3N_4 nanoparticles into the membrane matrix shows promising applications in terms of oil rejection and antifouling behaviour[6].

9. Leaching Studies

In order to confirm if the additive leaches out of the membrane during separation, leaching studies were carried out. On doing so it was evident that there was no Eg-C_3N_4 that was leached out of the membrane **(Fig S3)**. Hence, we can conclude that there is completely no EgC_3N_4 in the permeate solution and the intercalation of the additive into the membrane matrix is strong and stable when compared to few composite membranes[44] .

10. Perspective

The composite membranes fabricated are found to showcase enhanced hydrophilicity and porosity, owing to the additive added. The Eg-C_3N_4 additive due to its hydrophilic nature boosts the rate of water uptake and solvent exchange which has its direct influence on porosity and hydrophilicity of the composite membrane. The Eg-C_3N_4 duo exhibits a high oil-rejection tendency and high FRR compared to previous reported literature **(**Table 3**)** which paves way for its application in oil-in-water recovery. The slight compromise in pure water flux can be altered in future by chemical modifications of Eg-C_3N_4 which would enhance the surface functionality in turn modulating the water flux of the membrane.

Table 3
Comparison of Flux, Rejection and FRR on various membranes used in oil-water separation

Sl. no	Membranes	Flux (LMH)	Rejection (%)	FRR (%)	References
1	Uio-66-NH2@poly(acrylic acid) (PAA)	2330	99	80	45
2	MoS_2 and WS_2 hybrid poly(lactic acid) membrane	700	94.68	70	46
3	slippery liquid-infused polyethylene terephthalate membrane	~80	99.2	NA	47
4	polyzwitterion and bioinspired-adhesive polydopamine (PDA) modified CNTs	3400	99.5	95	48
5	Cu^{2+}/Alginate Multilayer Modified Membrane	1230	99.8	92.3	49
6	**Eg-C_3N_4-PSf**	**23.8**	**99.99%**	**99.4**	**Our Work**

Conclusion

A facile method of one pot synthesis was imbibed for the exfoliation of hydrophilic additive, g-C_3N_4 whose structural and chemical properties are evaluated using various analytical techniques. The membranes were synthesised using an elementary technique, nonsolvent induced phase separation. Evidence from FT-IR and XRD proved the chemical interaction between Eg-C_3N_4 and polymeric matrix and also evaluated the physical, mechanical and thermal stability of the composite membrane. On incorporation of this hydrophilic moiety into PSf membrane matrix, the composite membrane showed elevated oil rejection capacity of up to ~ 99.9% using 1g/L oil concentration as the initial feed concentration. On the other hand, the pristine PSf membrane showed two folds lesser oil rejection capacity compared to Eg-C_3N_4-PSf membrane. Membrane M_2 was found to show highest oil-water flux of 23.8 LMH followed by M_1 with a flux of 18.33 LMH and least for M_3 with a flux value of 17.5 LMH and the composite membranes showed oil rejection efficiency >99%. On carrying out fouling studies of the composite membranes it was found that the oil rejection potential of the membrane was never compromised. This feature of the membrane attributes to the enhanced shelf life or life time of the fabricated membrane. The FRR acts as a pillar for determining the membrane stability and efficiency of the membrane. It was found that all the three dosages were found to be satisfactory with M_1 membrane showing the highest FRR of 99.4%, which is quiet high compared to the literature survey and is well explained and in agreement with valley clogging theory and supported by AFM results of the membrane.

Declarations

Conflicts of interest

There are no conflicts to declare.

Acknowledgements

The authors thank the DST project (DST/TMD (EWO)/ OWUIS-2018/TS-05) for their financial support.

Author Contributions

Swathi Divakar: Methodology, investigation, article's layout and writing the original manuscript. **Prajwal Sherugar:** Reviewing and editing. **K.K. Nagaraja:** Characterisation techniques **Mahesh Padaki:** Reviewing, editing and funding acquisition and project co-administration. **R Geetha Balakrishna**: Supervision, reviewing, editing, funding acquisition and project administration.

Data Availability:

All data provided or analysed data during this study are included in this article and electronic supplementary information as mentioned in the manuscript.

References

1. Gupta, R. K., Dunderdale, G. J., England, M. W. & Hozumi, A. Oil/water separation techniques: A review of recent progresses and future directions. *J. Mater. Chem. A* **5**, 16025–16058 (2017).
2. Zhang, N. *et al.* A review on oil/water mixture separation material. *Ind. Eng. Chem. Res.* **59**, 14546–14568 (2020).
3. Statistics - ITOPF. https://www.itopf.org/knowledge-resources/data-statistics/statistics/.
4. Gao, H. *et al.* Switchable Wettability Surface with Chemical Stability and Antifouling Properties for Controllable Oil-Water Separation. *Langmuir* **35**, 4498–4508 (2019).
5. Deng, Y. *et al.* Metal-organic framework membranes: Recent development in the synthesis strategies and their application in oil-water separation. *Chem. Eng. J.* **405**, 127004 (2021).
6. Naik, N. S. *et al.* The efficient mixed matrix antifouling membrane for surfactant stabilized oil-in-water nanoemulsion separation. *J. Water Process Eng.* **32**, 100959 (2019).
7. Ali, N., Bilal, M., Khan, A., Ali, F. & Iqbal, H. M. N. Design, engineering and analytical perspectives of membrane materials with smart surfaces for efficient oil/water separation. *TrAC - Trends Anal. Chem.* **127**, (2020).
8. Serbanescu, O. S., Voicu, S. I. & Thakur, V. K. Polysulfone functionalized membranes: Properties and challenges. *Mater. Today Chem.* **17**, 100302 (2020).
9. Uragami, T. *2.10 Selective Membranes for Purification and Separation of Organic Liquid Mixtures*. *Comprehensive Membrane Science and Engineering* vol. 2 (Elsevier Ltd., 2017).
10. Cui, J., Qi, D. & Wang, X. Research on the techniques of ultrasound-assisted liquid-phase peeling, thermal oxidation peeling and acid-base chemical peeling for ultra-thin graphite carbon nitride nanosheets. *Ultrason. Sonochem.* **48**, 181–187 (2018).

11. Joshi, R. K. *et al.* Precise and ultrafast molecular sieving through graphene oxide membranes. *Science (80-.).* **343**, 752–754 (2014).
12. Sun, L., Huang, H. & Peng, X. Laminar MoS2 membranes for molecule separation. *Chem. Commun.* **49**, 10718–10720 (2013).
13. Wang, Y., Gao, B., Yue, Q. & Wang, Z. Graphitic carbon nitride (g-C3N4)-based membranes for advanced separation. *J. Mater. Chem. A* **8**, 19133–19155 (2020).
14. Alias, N. H. *et al.* Photocatalytic degradation of oilfield produced water using graphitic carbon nitride embedded in electrospun polyacrylonitrile nanofibers. *Chemosphere* **204**, 79–86 (2018).
15. Li, R. *et al.* Graphitic carbon nitride (g-C3N4) nanosheets functionalized composite membrane with self-cleaning and antibacterial performance. *J. Hazard. Mater.* **365**, 606–614 (2019).
16. Pattnaik, S. P., Behera, A., Acharya, R. & Parida, K. Green exfoliation of graphitic carbon nitride towards decolourization of Congo-Red under solar irradiation. *J. Environ. Chem. Eng.* **7**, 103456 (2019).
17. Mohamed, N. A. *et al.* Fabrication of exfoliated graphitic carbon nitride, (g-C3N4) thin film by methanolic dispersion. *J. Alloys Compd.* **818**, 152916 (2020).
18. Xu, J., Zhang, L., Shi, R. & Zhu, Y. Chemical exfoliation of graphitic carbon nitride for efficient heterogeneous photocatalysis. *J. Mater. Chem. A* **1**, 14766–14772 (2013).
19. Han, C., Wu, L., Ge, L., Li, Y. & Zhao, Z. AuPd bimetallic nanoparticles decorated graphitic carbon nitride for highly efficient reduction of water to H2 under visible light irradiation. *Carbon N. Y.* **92**, 31–40 (2015).
20. Vidyasagar, D. *et al.* 2D/2D Wg-C3N4/g-C3N4 composite as “Adsorb and Shuttle” model photocatalyst for pollution mitigation. *J. Photochem. Photobiol. A Chem.* **370**, 117–126 (2019).
21. Ghattavi, S. & Nezamzadeh-Ejhieh, A. GC-MASS detection of methyl orange degradation intermediates by AgBr/g-C3N4: Experimental design, bandgap study, and characterization of the catalyst. *Int. J. Hydrogen Energy* **45**, 24636–24656 (2020).
22. Challagulla, S., Payra, S., Chakraborty, C. & Roy, S. Determination of band edges and their influences on photocatalytic reduction of nitrobenzene by bulk and exfoliated g-C3N4. *Phys. Chem. Chem. Phys.* **21**, 3174–3183 (2019).
23. Miao, H., Zhang, G., Hu, X., Mu, J. & Han, T. A novel strategy to prepare 2D g-C 3 N 4 nanosheets and their photoelectrochemical properties *. *J. Alloys Compd.* **690**, 669–676 (2017).
24. Nadig, A. R., Naik, N. S., Padaki, M. & Pai, R. K. Journal of Water Process Engineering Impact of graphitic carbon nitride nanosheets in mixed- matrix membranes for removal of heavy metals from water. **41**, 1–11 (2021).
25. Mathialagan, A. *et al.* Fabrication and physicochemical characterization of g-C3N4/ZnO composite with enhanced photocatalytic activity under visible light. *Opt. Mater. (Amst).* **100**, 109643 (2020).
26. Mollahosseini, A., Rahimpour, A., Jahamshahi, M., Peyravi, M. & Khavarpour, M. The effect of silver nanoparticle size on performance and antibacteriality of polysulfone ultrafiltration membrane.

Desalination **306**, 41–50 (2012).

27. Sherugar, P., Padaki, M., Naik, N. S., George, S. D. & Murthy, D. H. K. Biomass-derived versatile activated carbon removes both heavy metals and dye molecules from wastewater with near-unity efficiency: Mechanism and kinetics. *Chemosphere* **287**, 132085 (2022).
28. Xu, C. *et al.* A polybenzimidazole/sulfonated graphite oxide composite membrane for high temperature polymer electrolyte membrane fuel cells. *J. Mater. Chem.* **21**, 11359–11364 (2011).
29. Singh, K. *et al.* Optical Resolution of Racemic Mixtures of Amino Acids through Nanofiltration Membrane Process. *Sep. Sci. Technol.* **49**, 2630–2641 (2014).
30. Wan, Z., Zhang, G., Wu, X. & Yin, S. Novel visible-light-driven Z-scheme Bi12GeO20/g-C3N4 photocatalyst: Oxygen-induced pathway of organic pollutants degradation and proton assisted electron transfer mechanism of Cr(VI) reduction. *Appl. Catal. B Environ.* **207**, 17–26 (2017).
31. Ma, Y. *et al.* Preparation and characterization of PSf/clay nanocomposite membranes with PEG 400 as a pore forming additive. *Desalination* **286**, 131–137 (2012).
32. Pereira, V. R., Isloor, A. M., Bhat, U. K. & Ismail, A. F. RSC Advances. 53874–53885 (2015) doi:10.1039/c5ra07994b.
33. Dong, Q., Liu, J., Yao, C. & Shao, G. Poly (vinyl alcohol) -Based Polymeric Membrane : Preparation and Tensile Properties. (2011) doi:10.1002/app.
34. Xie, H., Saito, T. & Hickner, M. A. Langmembran1. 4721–4727 (2011).
35. Nasseri, S., Ebrahimi, S., Abtahi, M. & Saeedi, R. Synthesis and characterization of polysulfone/graphene oxide nano-composite membranes for removal of bisphenol A from water. *J. Environ. Manage.* **205**, 174–182 (2018).
36. Su, Q. *et al.* Urea-derived graphitic carbon nitride as an efficient heterogeneous catalyst for CO2 conversion into cyclic carbonates. *Catal. Sci. Technol.* **4**, 1556–1562 (2014).
37. Padaki, M., Emadzadeh, D., Masturra, T. & Ismail, A. F. Antifouling properties of novel PSf and TNT composite membrane and study of effect of the flow direction on membrane washing. *Desalination* **362**, 141–150 (2015).
38. Lin, C. *et al.* Photocatalytic oxidation removal of fluoride ion in wastewater by g-C3N4/TiO2 under simulated visible light. *Adv. Compos. Hybrid Mater.* **4**, 339–349 (2021).
39. Tummons, E. *et al.* Membrane fouling by emulsified oil: A review. *Sep. Purif. Technol.* **248**, (2020).
40. Bagheripour, E. *et al.* Highly hydrophilic and antifouling nanofiltration membrane incorporated with water-dispersible composite activated carbon/chitosan nanoparticles. *Chem. Eng. Res. Des.* **132**, 812–821 (2018).
41. Zareei, F. & Hosseini, S. M. A new type of polyethersulfone based composite nanofiltration membrane decorated by cobalt ferrite-copper oxide nanoparticles with enhanced performance and antifouling property. *Sep. Purif. Technol.* **226**, 48–58 (2019).
42. An, Q., Li, F., Ji, Y. & Chen, H. Influence of polyvinyl alcohol on the surface morphology, separation and anti-fouling performance of the composite polyamide nanofiltration membranes. *J. Memb. Sci.* **367**,

158–165 (2011).
43. Vrijenhoek, E. M., Hong, S. & Elimelech, M. Influence of membrane surface properties on initial rate of colloidal fouling of reverse osmosis and nanofiltration membranes. **188**, 115–128 (2001).
44. Yong, L., Wahab, A., Peng, C. & Hilal, N. Polymeric membranes incorporated with metal / metal oxide nanoparticles : A comprehensive review. *DES* **308**, 15–33 (2013).
45. Cao, J. *et al.* Self-assembled MOF membranes with underwater superoleophobicity for oil/water separation. *J. Memb. Sci.* **566**, 268–277 (2018).
46. Krasian, T., Punyodom, W. & Worajittiphon, P. A hybrid of 2D materials (MoS2 and WS2) as an effective performance enhancer for poly(lactic acid) fibrous mats in oil adsorption and oil/water separation. *Chem. Eng. J.* **369**, 563–575 (2019).
47. Zhao, X. *et al.* Bioinspired synthesis of polyzwitterion/titania functionalized carbon nanotube membrane with superwetting property for efficient oil-in-water emulsion separation. *J. Memb. Sci.* **589**, 117257 (2019).
48. Zhao, L. *et al.* Antifouling slippery liquid-infused membrane for separation of water-in-oil emulsions. *J. Memb. Sci.* **611**, 118289 (2020).
49. Gao, S. *et al.* Layer-by-Layer Construction of Cu2+/Alginate Multilayer Modified Ultrafiltration Membrane with Bioinspired Superwetting Property for High-Efficient Crude-Oil-in-Water Emulsion Separation. *Adv. Funct. Mater.* **28**, 1–11 (2018).

Figures

Figure 1

a) XRD b) FTIR, c) and d) pores size distribution and BET isotherm of exfoliated g-C_3N_4

Figure 2

a) and b) are the FESEM images of bulk and exfoliated g-C_3N_4 respectively

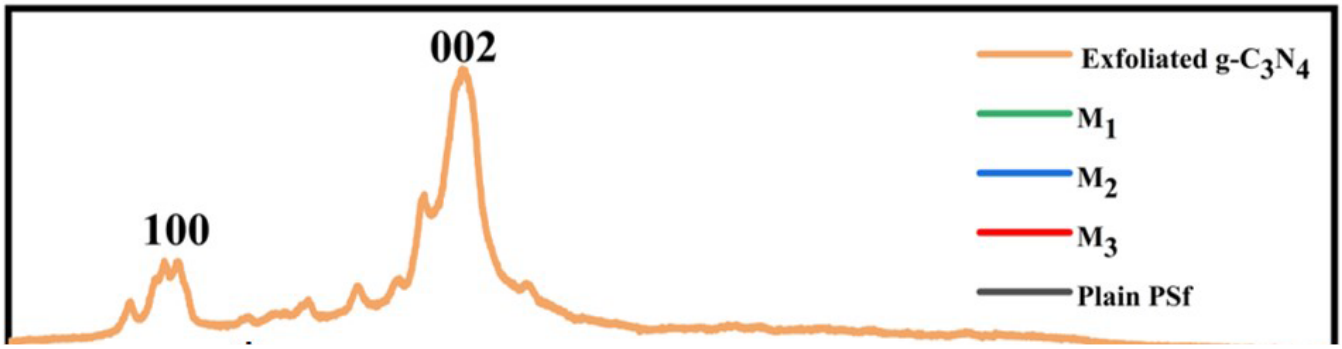

Figure 3

XRD pattern of Eg-C_3N_4, plain PSf, M_1, M_2 and M_3 membranes

Figure 4

ATR-IR spectra of plain PSf, M_1, M_2, M_3 and Eg-C_3N_4

Figure 5

Interactions between exfoliated graphitic carbon nitride and polysulphone

Figure 6

FESEM images of plain PSf, M_1, M_2 and M_3 membranes

Figure 7

Atomic Force Microscopic (AFM) images of a) PSf, b) M_1, c) M_2 and d) M_3

Figure 8

Zeta Potential of plain PSf, M_1, M_2 and M_3 membranes

Figure 9

Thermogravimetry analysis curve of plain PSf, M_1, M_2 and M_3 membranes

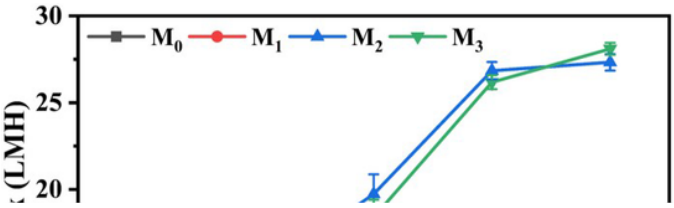

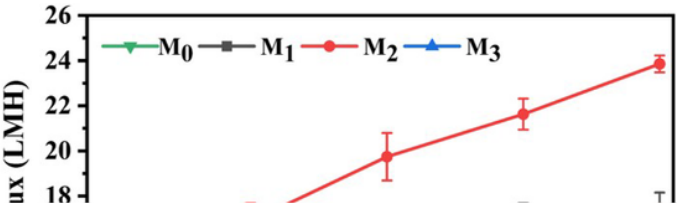

Figure 10

Pure water and Oil-water flux of plain PSf (M_0), M_1, M_2 and M_3

Figure 11

Oil-water Emulsion droplet size

Figure 12

Oil rejection efficiency of plain PSf, M_1, M_2 and M_3 membranes at various pressures

Figure 13

Antifouling Studies of M1, M2 and M3 membranes

Figure 14

Long term Oil rejection Studies

Supplementary Files

This is a list of supplementary files associated with this preprint. Click to download.

- GraphicalAbstract.png
- SupplementaryInformation.rtf